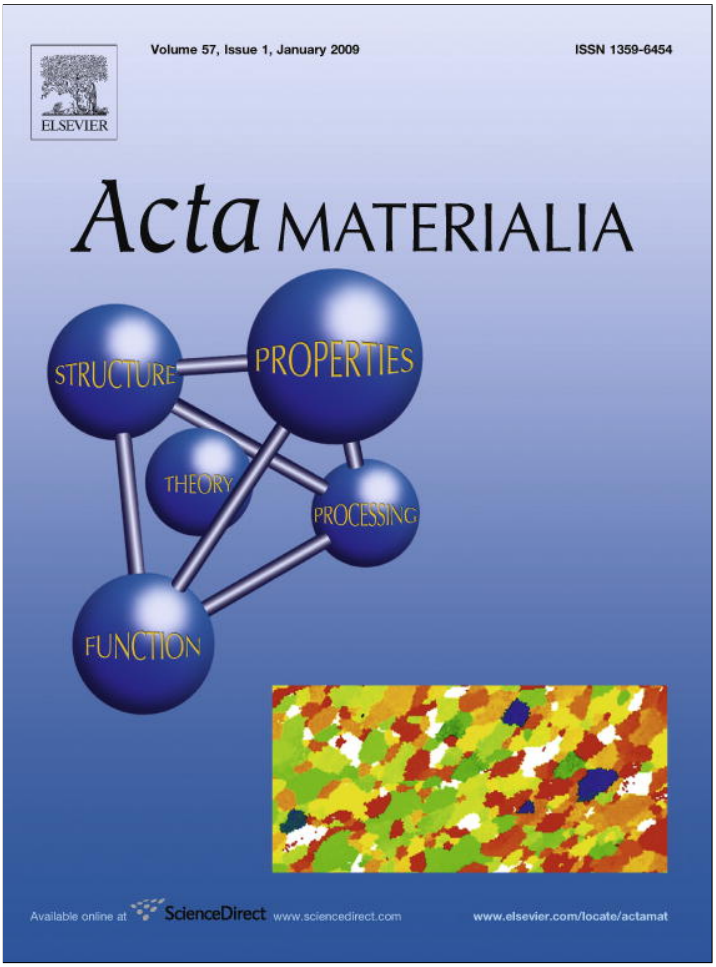

Available online at www.sciencedirect.com
ScienceDirect
Acta Materialia 57 (2009) 224–231
Acta MATERIALIA
www.elsevier.com/locate/actamat

First-principles study of vacancy formation and migration in clean and Re-doped γ'-Ni_3Al

Xu Zhang [a,*], Chong-Yu Wang [a,b]

[a] Department of Physics, Tsinghua University, Beijing 100084, China
[b] The International Centre for Materials Physics, Chinese Academy of Sciences, Shenyang 110016, China

Received 13 April 2008; received in revised form 28 August 2008; accepted 30 August 2008
Available online 1 October 2008

Abstract

Using density functional theory calculations in conjunction with the climbing images nudged elastic band method, we studied the vacancy formation and migration in clean and Re-doped Ni_3Al. Both the chemical potential of the species and the magnetic effect are considered to determine the vacancy formation energy. We also simulated the vacancy migration in a complete set of migration paths. The evaluated vacancy formation energy and activation energy for the motion of vacancy compared well with the experimental results. Also, the obtained migration ways for the diffusion of Ni and Al atoms are consistent with previous theoretical predictions and experimental observations. Magnetism is found to influence both the vacancy formation and migration. Our results reveal that Re doping can inhibit the formation of Ni vacancies but facilitate the formation of Al vacancies, and can also inhibit the migration of neighboring vacancies. While the doped Re atom on the Al site is stable, the Re atom on the Ni site can diffuse within the Ni-sublattice mediated by Ni vacancies.

Keywords: Nickel alloys; Bulk diffusion; Vacancies; Ab initio electron theory

1. Introduction

Ni-based superalloy, where the main macrostructure of such alloys is the $L1_2$ intermetallic compound Ni_3Al (the γ' precipitate) that is coherent with an Ni-based solid solution (the γ matrix), is a promising high-temperature structural material with excellent mechanical properties. γ'-Ni_3Al is still a major focus of interest due to its increasing yield strength as a function of increasing temperature and elevated temperature creep strength. Experiments [1–4] have shown that by properly increasing the concentration of the alloying element Re in both the γ and γ' phases, the high-temperature mechanical properties of such a material can be drastically improved. For the intermetallic compounds, the nature of the point defect is important for understanding and controlling the physical and mechanical properties of the materials. In particular, in the investigation of creep behavior at high temperature, the diffusion of vacancy and its activation energy (the sum of formation and migration energies) play an important role in the simple Nabarro–Herring creep model [5] and the classic dislocation climb theory [6]. Thus, knowledge about the formation and migration of vacancy and the effect of doped Re in the γ' phase is useful for understanding the mechanical properties and its strengthening effect in the Ni-based superalloy.

Over the past few decades, the formation and diffusion of point defects in Ni_3Al have been studied extensively by a large body of experimental and theoretical works. Thermodynamical properties of point defects, such as vacancies or antisite atoms in Ni_3Al, have been investigated using positron annihilation studies [7,8]. The diffusion data of Ni_3Al studied by radiotracer and interdiffusion experiments are summarized in Refs. [9–12]. First-principles calculations [13] and atomistic simulations [14,15] have been

* Corresponding author.
E-mail address: zx00@mails.tsinghua.edu.cn (X. Zhang).

1359-6454/$34.00 © 2008 Acta Materialia Inc. Published by Elsevier Ltd. All rights reserved.
doi:10.1016/j.actamat.2008.08.052

used to evaluate the vacancy formation energy in Ni_3Al. The diffusion of point defects in Ni_3Al has also been studied by using molecular dynamics with empirical interatomic potential [16–18]. Despite these efforts, theoretical data about the effect of magnetism and dopants on the vacancy formation and migration are still lacking. Therefore, a systematically theoretical investigation is desirable in order to obtain more fundamental insights on the subject.

In this paper, we employ density functional theory (DFT) calculations to study the formation energy and migration paths and barriers for vacancy as well as the effect of Re doping.The chemical potential of species is evaluated as an important parameter for determining the formation energy of vacancy. The complete set of migration paths to the first and second nearest neighbors has been derived for the $L1_2$ lattice taking into account the diffusion of vacancies and atoms in Ni_3Al. Previous studies [19,20] have shown that the perfect Ni_3Al has weak itinerant ferromagnetism. To consider the magnetism of point defects, we also perform spin-polarized calculations for vacancy formation and migration. The formation energy of vacancy and energy barriers of various migration paths under all possible occupational sites of the doped Re are evaluated to study the effect of Re doping on the vacancy formation and migration.We analyze the migration of the doped Re atom mediated by vacancies, and present the stable occupational site of the doped Re and the most effective way for the diffusion of Re atom.

This paper is organized as follows. In Section 2, we describe the computational framework and the complete set of migration paths for vacancies, as well as the occupational sites of the doped Re atom. Then we present our calculated results and analysis in Section 3, which is divided into four subsections. In the first two subsections, we study the vacancy formation and migration in clean Ni_3Al. The magnetic effects are analyzed in the third subsection. The influence of Re doping on the vacancy formation and migration is presented in the last subsection. Finally, a short summary is given in Section 4.

2. Details of the calculations

2.1. Computational method

Calculations within density functional theory were performed with the Vienna Ab Initio Simulation Package [21] (VASP) using the projector augmented wave (PAW) method [22] and the generalized gradient approximation (GGA) in the parametrization by Perdew and Wang (PW91) [23]. We also used the spin-polarized GGA (SGGA) to include magnetic effects. A plane-wave cutoff of 280 eV was used in the calculations which yields well converged results. The convergence accuracy of total energy was chosen as 10^{-5} eV in the relaxation of electronic degrees of freedom. For the primitive unit cell of Ni_3Al, the k points were sampled according to Monkhorst–Pack scheme [24] with $11 \times 11 \times 11k$ mesh. The calculated lattice constant a_0 and bulk modulus by GGA (SGGA) were 3.570 Å (3.571 Å) and 179 GPa (179 GPa), respectively, which compared well with the experimental values of 3.57 Å [25] and 174 GPa [26].

Crystals with defects (vacancy and/or Re doping) were modeled using supercells $3a_0 \times 3a_0 \times 3a_0$ (containing 108 atoms), which are large enough to get converged total energies according to our tests. A $3 \times 3 \times 3k$ mesh was used for the k points sampling. The defects were seated at the center of the supercell, and the structure was then relaxed by minimizing the total energy with a convergence accuracy of 10^{-4} eV. To obtain the transition state and energy barriers of vacancy migration, we employed the climbing image nudged elastic band method (CI-NEB) [27,28] as implemented in VASP by Henkelman, Jónsson et al. [29]. Since the determination of the minimum energy path and the saddle point works reliably for a small number of images by CI-NEB [27,28,30], we used four images in the computations for various migration paths. The images were relaxed until the maximum residual force was less than 10 meV/Å.

2.2. Migration paths

The possible migration paths via first as well as second nearest neighbors are schematically shown in Fig. 1. $L1_2$ structure can be decomposed into two sublattices, α and β, occupied by Ni atoms and Al atoms, respectively. A site of the β-sublattice is surrounded by 12 nearest neighbors located on the α-sublattice, whereas a site of the α-sublattice is surrounded by four sites of the β-sublattice and eight sites of the α-sublattice. We first consider the vacancy migration on the same sublattice. Among the jumps of Al vacancy V_β to the first nearest Al site, there are six symmetry equivalent paths, e.g. A1 → A2 shown in Fig. 1. Since A1 → A2 and A2 → A1 are equivalent, we use A1 ↔ A2 to denote these migration paths. Here, we exclude the

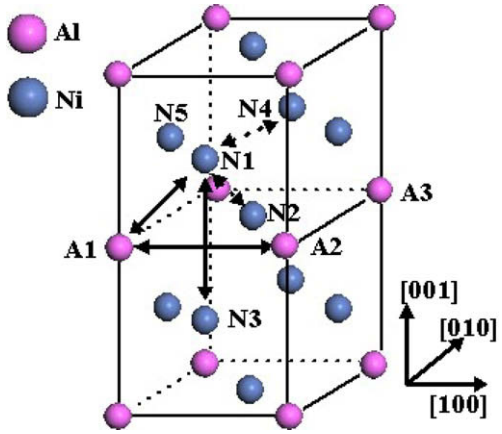

Fig. 1. Migration paths accessible to Al and Ni vacancies on the $L1_2$ lattice via jumps to the first or second nearest neighbor sites. The arrows denote the migration paths.

migration of V_β to the second nearest Al site (e.g. A1 ↔ A3 in Fig. 1) due to the fact that the Al atom needs to pass through a triangle consisting of three nearest neighbor Ni atoms (e.g. N1, N2 and N5 in Fig. 1) where the energy barrier is much higher, suggesting that this migration is unfavorable. Similarly, we have the migration paths of Ni vacancy V_α on the α-sublattice, N1 ↔ N2, N1 ↔ N3 and N1 ↔ N4, which have eight, four and two symmetry equivalent paths, respectively. Next, antisite mediated vacancy migrations were considered, which involve the migration between two sublattices, αβ- or βα-jump. For example, in the path that V_β jumps to the first nearest neighbor Ni site of the α-sublattice (A1 → N1), the final state has a V_α associated with an antisite Ni_β, which is denoted by $\{Ni_\beta + V_\alpha\}$.

To study the effect of Re doping on the vacancy migration, the doped site was chosen such that the distance between it and the migration path was at a minimum. As an example, for the Re-doped Al site (e.g. A1 in Fig. 1) Re_β, we calculate the migration paths, V_β-jump A2 ↔ A3, V_α-jump N1 ↔ N2 and N1 ↔ N3, as well as αβ- and βα-jump N1 → A2 and A2 → N1. Similarly, we can model all possible migration paths under the Re-doped Ni site Re_α. Three migration paths via which Re jumps to the first nearest vacancy site, $Re_\alpha \to V_\alpha$, $Re_\beta \to V_\beta$ and $Re_\alpha \to V_\beta$ (its inverse migration path is $Re_\beta \to V_\alpha$), were calculated to simulate the diffusion of doped Re atom mediated by vacancies.

3. Results and discussion

3.1. Vacancy formation energy

The vacancy formation energy is defined as the energy needed to remove an atom from the host material and place it into a reservoir of the same atomic species. There are two factors affecting the vacancy formation energy. First, the energy needed to take one atom away from the host depends on the interaction of this atom with others. For species j, it is calculated by

$$\Delta\chi(j) = E_{tot}(Ni_3Al,[j]) + E_{tot}(j) - E_{tot}(Ni_3Al) \quad (1)$$

where $E_{tot}(Ni_3Al)$ and $E_{tot}(Ni_3Al,[j])$ are the total energies of the perfect Ni_3Al solid and the solid containing one j-species vacancy, respectively. $E_{tot}(j)$ is the total energy per atom in j-species elemental solid. Another factor is the chemical potential of the atomic reservoir, which is a critical quantity for controlling the defect concentration [31,32]. The chemical potential is defined as the Gibbs free energy per atom in the atomic reservoir [33]. The energy per atom in elemental solid of equilibrium is often taken as the reference energy for describing the chemical potential in studies of defect physics [34,35]. A higher chemical potential implies a greater energy cost in moving atoms into the reservoir and hence a large vacancy formation energy.

Next, we determine the chemical potentials in the Ni_3Al solid phase. When Ni and Al elements are mixed chemically to form Ni_3Al compounds, the formation enthalpy ΔH is given by $\Delta H(Ni_3Al) = E_{tot}(Ni_3Al) - 3E_{tot}(Ni) - E_{tot}(Al)$. In the equilibrium state, the total energy for Ni_3Al in the solid phase of $L1_2$ and the total energy for these atoms in reservoirs should be equal. So the equilibrium condition is given by [31]

$$3\mu_{Ni} + \mu_{Al} = \Delta H(Ni_3Al) \quad (2)$$

where μ_j is the chemical potential of species j (here j represents Ni or Al). Furthermore, the energy of atoms in reservoir must be less than the energy in the secondary phase to prevent the Ni and Al atoms in reservoirs from precipitating into the elemental solid, which is the secondary phase [31,32],

$$\mu_{Ni} \leqslant 0, \quad \mu_{Al} \leqslant 0 \quad (3)$$

With Eqs. (2) and (3), ranges for chemical potentials μ_{Ni} and μ_{Al} can be determined by

$$\begin{aligned} &\frac{\Delta H(Ni_3Al)}{3} \leqslant \mu_{Ni} \leqslant 0, \\ &\Delta H(Ni_3Al) \leqslant \mu_{Al} \leqslant 0 \end{aligned} \quad (4)$$

Finally, the vacancy formation energy $E_v^F(j)$ of species j can be obtained by

$$E_v^F(j) = \Delta\chi(j) + \mu_j \quad (5)$$

The computed vacancy formation energies are summarized in Table 1. Here we use the results calculated by SGGA to discuss the vacancy formation energy. Considering that $L1_2$ Ni_3Al is formed under the Ni-rich condition, we have $\mu_{Ni} \simeq 0$ eV and $\mu_{Al} \simeq \Delta H = -1.79$ eV. The formation energies of V_α and V_β are then 1.59 and 1.80 eV, respectively. The average vacancy formation energy can be obtained by [36]

$$E_{av}^F = \frac{N_{Ni}E_v^F(Ni) + N_{Al}E_v^F(Al)}{N_{Ni} + N_{Al}} \quad (6)$$

where N_{Ni} and N_{Al} are numbers of V_α and V_β, respectively. And in thermal equilibrium there are

Table 1
Calculated vacancy formation energies (in eV) of species j in clean Ni_3Al

	V_α		V_β	
	GGA	SGGA	GGA	SGGA
$\Delta\chi$	1.61	1.59	3.68	3.59
E_v^F	[0.97, 1.61]	[1.00, 1.59]	[1.75, 3.68]	[1.80, 3.59]
	Under the condition of $\mu_{Ni} = 0$ eV			
E_v^F	1.61	1.59	1.75	1.80
c_v (300 K)	3.9×10^{-27}	8.4×10^{-27}	5.9×10^{-30}	8.6×10^{-31}
c_v (1400 K)	5.1×10^{-6}	6.0×10^{-6}	5.2×10^{-7}	3.5×10^{-7}

$\Delta\chi$ is the formation energy needed for vacancy creation under the condition of $\mu_j = 0$. The formation energy E_v^F is within a range which is given in brackets with two boundary values. The equilibrium concentration of vacancies c_v (per site) at room temperature (300 K) and work temperature (1400 K) are estimated by the vacancy formation energies under the condition of $\mu_{Ni} = 0$ eV.

$$\frac{N_{Ni}}{N_{Al}} = \frac{g_{Ni}}{g_{Al}} \exp\left(-\frac{E_v^F(Ni) - E_v^F(Al)}{k_B T}\right) \quad (7)$$

where g_{Ni} and g_{Al} are known stoichiometric coefficients of the Ni_3Al compound. Since $E_v^F(Al) > E_v^F(Ni)$, $g_{Ni}/g_{Al} < N_{Ni}/N_{Al} < \infty$. We can then determine the range of the average vacancy formation energy as being 1.59 eV $< E_{av}^F <$ 1.64 eV, which compares well with the experimental results of 1.62 eV [37] and 1.6 ± 0.2 eV [7].

3.2. Vacancy migration in clean Ni_3Al

A summary of the calculated migration barriers is presented in Table 2. First, we consider the migration of V_α and the diffusion of Ni atoms. V_α jumps to the first nearest neighbor site within the α-sublattice by crossing a barrier of 0.97 eV, which is approximately 0.2 eV lower compared with the experimental result (1.2 ± 0.2 eV [7]). Thus Ni atoms can easily diffuse via nearest neighbor jumps on its own sublattice mediated by thermal vacancies V_α. It is hard for V_α to jump to the second nearest neighbor site, as elevated barriers larger than 3.0 eV need to be crossed. Another way an Ni atom might jump is via the migration path A1 → N1 due to the low barrier of 0.95 eV, which makes an antisite Ni_β. However, the probability of this is expected to be small because of the order–disorder transition of Ni_3Al [38]. The diffusion of Ni in Ni_3Al is therefore likely to be mostly due to the migration of Ni atoms within their own sublattice, which is consist with experimental observations [39]. The evaluated activation energy of Ni diffusivity is about 2.6 eV compared with the experimental report of 3.0 eV [10].

V_β cannot jump effectively to the first nearest Al site within th eβ-sublattice due to the high migration barrier of 3.33 eV. It is therefore improbable that Al will diffuse on its own sublattice. However, the migration path N1 → A1, with energy barrier of 1.00 eV, allows Al atoms to move to the α-sublattice and form antisites Al_α. This suggests that the diffusion of Al atoms may be more effective by using the α-sublattice, which is supported by previous theoretical studies as well as experimental works [18,40]. However, one should note that the diffusion of Al atoms via the α-sublattice will create disordering in Ni_3Al. Two mechanisms have been proposed so far to account for this type of diffusion. One is the so-called 6-jump cycle [41]. Once a 6-jump cycle is completed, the Al atom moves to the first nearest Al site and the crystal is ordered anew, which enables the Al atom to migrate over long distances without altering the long-range degree of order in Ni_3Al. The other mechanism is the well-known 5-jump frequency model [40], where Al atoms diffuse over long distances in the antisite position via exchanges of the antisite atom with a nearest vacancy on the α-sublattice. In this respect, the Al_α antisite plays a role similar to substitutional impurities on the α-sublattice.

With the evaluated energy barriers, we could estimate the diffusion frequency for the vacancy migration by an Arrhenius law: [42]

$$\Gamma_v^M = \Gamma_0 \exp[-\Delta G_v^M / k_B T] \quad (8)$$

where the attempt frequency Γ_0 is usually approximated by a characteristic frequency such as the Debye frequency [30], which yields $\Gamma_0 \approx 10$ THz for Ni_3Al. ΔG_v^M is the free enthalpy of migration which consists of the migration enthalpy and the contribution of migration entropy. The migration enthalpy most crucially affects the diffusion frequency [30]. We thus replace ΔG_v^M by E_v^M in Eq. (8) to estimate the diffusion frequency. The results are presented in Table 2.

3.3. Magnetic effects on vacancy formation and migration

Here, we employ the calculated spin polarization and angular momentum decomposed density of states (*s*-, *p*- and *d*-DOS) to analyze the magnetic effects on vacancy formation and migration. For perfect Ni_3Al, our results reveal that the spin polarization comes dominantly from the Ni *d* electrons (0.68 μ_B from three Ni atoms), while the Ni *s*, *p*, Al *s*, *p* electrons are polarized slightly negatively (−0.03 μ_B), to give rise to a total magnetic moment of 0.65 μ_B per unit cell. Comparing the magnetic moment of pure Ni, 2.42 μ_B per unit cell, the polarization of *d* electrons in Ni_3Al is reduce by about two-thirds due to hybridization with the Al *p* electrons, as shown in Fig. 2(a)–(c).

The calculations by GGA and SGGA yield the same lattice constant, bulk modulus and cohesive energy for perfect

Table 2
Energy barriers E_v^M and diffusion frequency Γ_v^M (at 1400 K) for vacancy migration

Migration path	E_v^M (eV)		Γ_v^M (s^{-1})	$E_f - E_i$ (eV)		$M_s - M_i$ (μ_B)	$M_f - M_i$ (μ_B)
	GGA	SGGA	SGGA	GGA	SGGA	SGGA	
A1 ↔ A2	3.27	3.33	≈0	0	0	−1.06	0
N1 ↔ N2	0.93	0.97	3.3×10^9	0	0	−1.16	0
N1 ↔ N3	3.63	3.69	≈0	0	0	−1.81	0
N1 ↔ N4	3.59	3.68	≈0	0	0	−4.25	0
A1 → N1	0.89	0.95	3.9×10^9	−0.01	0.02	−0.76	−0.51
N1 → A1	1.00	1.00	2.6×10^9	0.70	0.70	−0.12	−0.27

$E_f - E_i$ ($M_f - M_i$) denotes the difference of the total energy (magnetic moment) between the final state and initial state, which is non-zero for the vacancy migration associated with antisite. The definition of migration paths can be seen in Fig. 1 and Section 2. $M_s - M_i$ is the difference of magnetic moment between the saddle point state and the initial state.

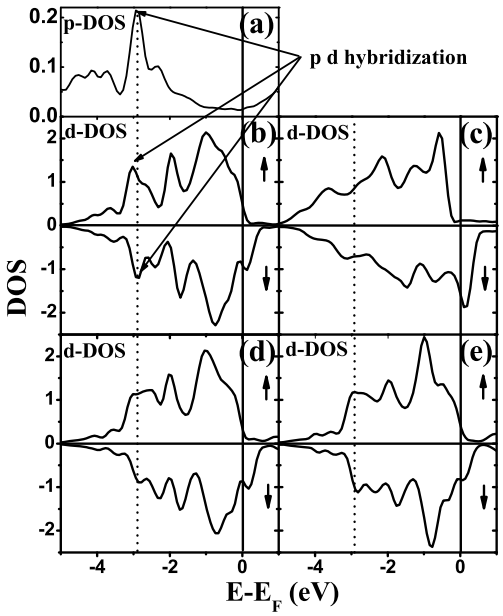

Fig. 2. (a) *p*-DOS of an Al atom in perfect Ni_3Al, (b) *d*-DOS of an Ni atom in perfect Ni_3Al, (c) *d*-DOS of an Ni atom in pure Ni solid, (d) *d*-DOS of an Ni atom which is in the first shell around vacancy V_β, and (e) *d*-DOS of an Ni atom which is in the first shell around vacancy V_α. The Fermi energy level is shifted to zero. The *d*-DOS has two parts, one is spin up and the other is spin down.

Ni_3Al. However, as can be seen from Table 1, the difference of $\Delta\chi$(Ni) ($\Delta\chi$(Al)) calculated by GGA and SGGA is 0.02 eV (0.09 eV) for V_α (V_β). The magnetic effect should therefore be considered for systems containing vacancy defects. To show the magnetic effect on the vacancy, we give the magnetization density of V_α and V_β in Fig. 3. It can be seen that V_β induces an accumulation of magnetization density on the Ni atoms of the first shell around the vacancy. As shown in Fig. 2(d), the *p–d* hybridization is weakened due to the formation of V_β, which increases the spin polarization of *d* electrons of the neighboring Ni atoms accordingly. The numerical results reveal that a localized magnetic moment 2.15 μ_B is formed due to V_β. However, the influence of V_α on the magnetization density can be negligible according to Fig. 3b. The DOS (Fig. 2(e)) also shows that the *p–d* hybridization is slightly influenced by the formation of V_α. Therefore, the magnetism has explicitly influenced the vacancy formation energy for V_β, while this influence is much smaller for V_α.

Comparing the migration barriers calculated by GGA and SGGA, the energy barriers are seen to be underestimated when the magnetic effect is not considered. We have evaluated the variation of the magnetic moment in the transition state during the vacancy migration. Table 2 presents the difference in the magnetic moment between the saddle point state and initial state. As can be seen in Table 2, the magnetic moment decreases in the transition state with the migration barrier being elevated. The greater the decrease in the magnetic moment, the greater the increase in the energy barrier. We find that mechanisms that decrease of magnetic moment differ between the V_α and V_β migrations. As shown in Fig. 4, the *p–d* hybridization becomes stronger during the migration of V_β, which reduces the spin polarization of the *d* electrons of the neighboring Ni atoms. As a result, the localized magnetic moment induced by a vacancy is reduced in the transition state of V_β migration. However, in the transition state of V_α migration (we take the migration path N1 ↔ N4 as an example), as can be seen in Fig. 5, the direction of spin polarization is inverted for the diffused Ni atom, and the spin polarization of the neighboring Ni atoms become zero due to the *d* electrons hybridizing strongly with the *s* electrons of the diffused Ni atom. Thus the magnetic moment around the diffused Ni atom become smaller during the migration of V_α.

3.4. Vacancy formation and migration with Re doping

In this subsection, we use defect grand canonical (GC) formation energies to study the effect of Re doping on the vacancy formation. The GC formation energy of a given defect *d*, $\tilde{E}(d)$, is calculated in the usual way as [43]

$$\tilde{E}(d) = E(d) - E_0 \tag{9}$$

where $E(d)$ and E_0 is the energy of a large supercell with and without the defect considered, respectively. The higher

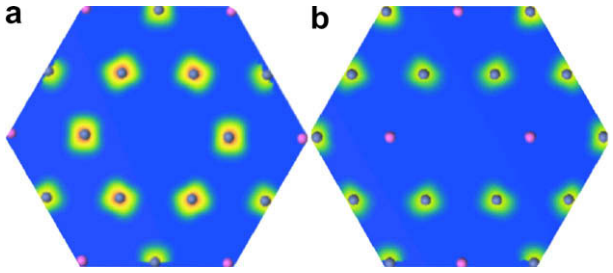

Fig. 3. The calculated magnetization density ($\rho_\uparrow(\mathbf{r}) - \rho_\downarrow(\mathbf{r})$ in $Å^{-3}$) for (a) V_β and (b) V_α in the (1 1 1) plane. The contour scale ranges from 0 (blue) to 0.69 (red). (For interpretation of the references to color in this figure legend, the reader is referred to the web version of this article.)

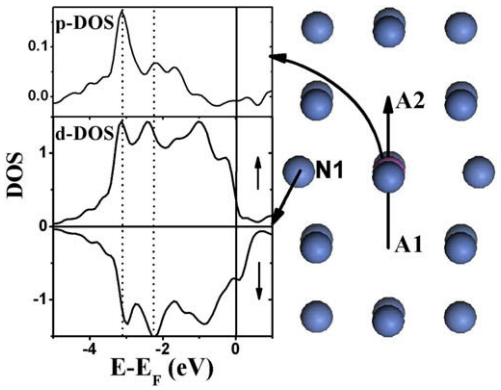

Fig. 4. *p*-DOS of the diffused Al atom and *d*-DOS of an Ni atom which is first nearest neighbor of the diffused Al atom, in the saddle point state of the migration path A1 ↔ A2.

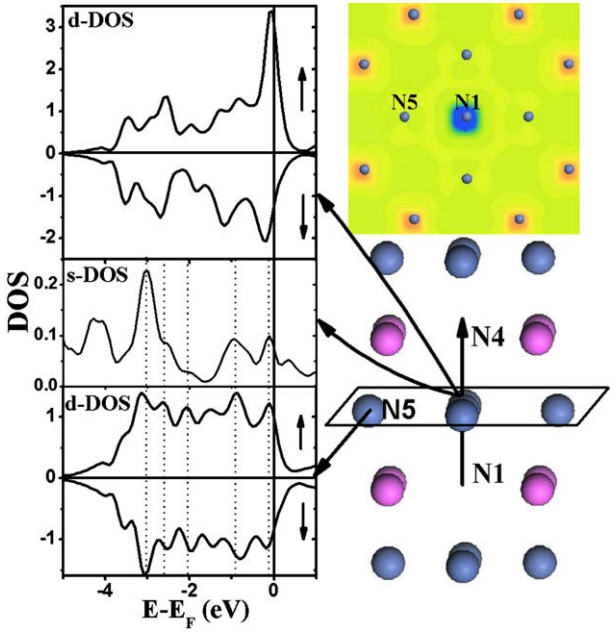

Fig. 5. *s*-DOS and *d*-DOS of the diffused Ni atom, and *d*-DOS of an Ni atom which is the first nearest neighbor of the diffused Ni atom, in the saddle point state of the migration path N1 ↔ N4. The top right figure shows the magnetization density (in Å^{-3}) in the (010) plane which is perpendicular to the migration path. The contour scale ranges from −0.40 (blue) to 0.40 (red). (For interpretation of the references to color in this figure legend, the reader is referred to the web version of this article.)

the GC formation energy, the harder the formation of the defect. One should be noted that the vacancy formation energy rather than the GC formation energy determines the concentration of vacancies. GC energies can be easily extended to take into account defect interactions (di-defects, tri-defects, etc.). For the system containing several defects, the energy of the system reads $E = E_0 + \sum_d \tilde{E}(d)$, where the d index runs over the defects. We can then obtain the GC formation energies of vacancies (V_α or V_β) under Re doping (Re_α or Re_β), $\tilde{E}(V_{\alpha,\beta}|Re_{\alpha,\beta})$, as

$$\tilde{E}(V_{\alpha,\beta}|Re_{\alpha,\beta}) = E(V_{\alpha,\beta} + Re_{\alpha,\beta}) - \tilde{E}(Re_{\alpha,\beta}) - E_0 \qquad (10)$$

where $E(V_{\alpha,\beta} + Re_{\alpha,\beta})$ is the energy of the system containing a vacancy and an Re doping, and $\tilde{E}(Re_{\alpha,\beta})$ is the defect GC energy of Re doping. According to the calculated GC formation energies (in Table 3), the Re doping slightly increase the GC formation energy of V_α, and it induces a larger decrease in the GC formation energy of V_β. Consequently, the formation of an Al vacancy is easier around the Re doping than in clean Ni_3Al. In addition, the Re doping can slightly inhibit the formation of Ni vacancy.

Table 3
The calculated GC formation energy (in eV) of vacancy in clean and Re-doped Ni_3Al

	$\tilde{E}$(V) (clean)	$\tilde{E}$(V|Re$_\alpha$)	$\tilde{E}$(V|Re$_\beta$)
V_α	6.98	7.02	7.09
V_β	7.33	6.93	7.22

The vacancy is chosen at the first nearest site of the doped Re atom.

To study the effect of Re doping on the vacancy migration, we calculate the minimum energy paths for various vacancy migrations with Re doping, as shown in Fig. 6. It can be seen that the Re doping, Re_α and Re_β have systematically increased the energy barriers of the vacancy migration. According to the analysis in the previous subsection, vacancies on the α-sublattice can move effectively within their own sublattice, and vacancies on the β-sublattice use the α-sublattice for diffusion via $\beta\alpha$-jump. Here we concentrate the effect of Re doping on the above two vacancy migrations, where the first one corresponds to Fig. 6b and the latter corresponds to Fig. 6e. First, for the migration of V_α within the α-sublattice, Re_α and Re_β increase the energy barrier by 0.04 and 0.08 eV, respectively. Second, the migration barrier of V_β jumping to the α-sublattice is elevated by 0.10 and 0.20 eV for Re_α and Re_β, respectively. In this migration path, the doping types Re_α and Re_β lead to different final states. While the doping type Re_α induces a more stable final state $\{Ni_\beta + V_\alpha\}$ which is 0.14 eV lower than the initial state $\{V_\beta\}$, Re_β causes the opposite effect, so that the final state is a metastable state which is 0.13 eV higher than the initial state. This means that Re_α may facilitate V_β jumping to the α-sublattice and Re_β can inhibit this jumping. In the following discussion, we have revealed that Re_β is much more stable than

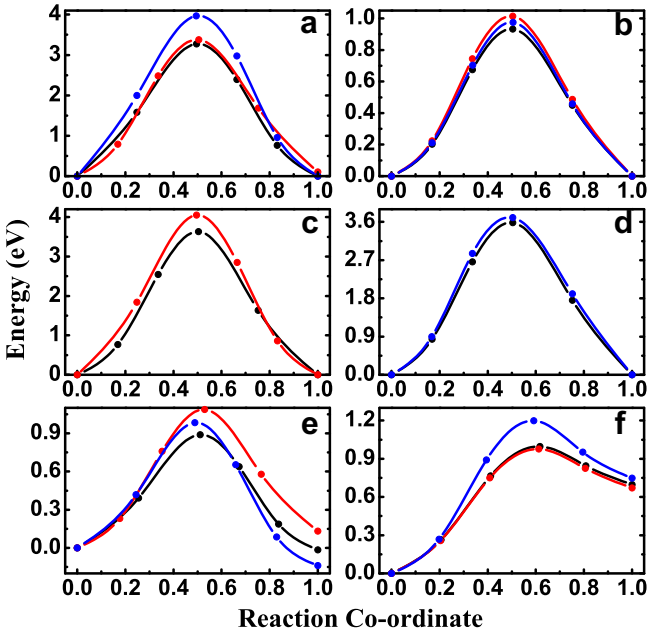

Fig. 6. CI-NEB calculations of the minimum energy path for vacancy migration in clean and Re-doped Ni_3Al by using GGA. The initial and final states correspond to reaction coordinates of 0.0 and 1.0, respectively. The black, blue and red solid lines denote the vacancy migration in clean, Re_α-doped and Re_β-doped Ni_3Al, respectively. The migration paths correspond to (a) A1 ↔ A2, (b) N1 ↔ N2, (c) N1 ↔ N3, (d) N1 ↔ N4, (e) A1 → N1 and (f) N1 → A1. (For interpretation of the references to color in this figure legend, the reader is referred to the web version of this article.)

Re_α. Thus the Re doping (Re_β is favorable) can inhibit the migrations of its neighboring vacancies.

We have shown that Re doping increases the formation energy and migration barrier of an Ni vacancy whose migration is the dominant way in which vacancies diffuse in Ni_3Al. The Re doping could thus inhibit the formation and migration of the most effectively diffused vacancies, which accordingly elevates the creep strength of Ni_3Al based on the classic dislocation climb theory [6].

Finally, we consider the diffusion of doped Re atoms mediated by vacancies. The evaluated energy barrier is 1.00 eV for Re_α jumping to the first nearest V_α on the α-sublattice. For the diffusion on the β-sublattice, an Re atom hopping to the first nearest V_β needs to cross a much larger barrier, of 5.07 eV. Re_β hops to the first nearest V_α via a $\beta\alpha$-jump by crossing a energy barrier of 2.24 eV. The final configuration is a metastable state which is 1.62 eV higher than the initial state. As an inverse migration path, the metastable configuration $\{Re_\alpha + V_\beta\}$ only needs to cross a barrier of 0.62 eV to reach the stable configuration $\{Re_\beta + V_\alpha\}$. Based on these calculated results, we can conclude that Re doping is stable when locating on the β-sublattice, and the migration of Re_α within the α-sublattice mediated by vacancies V_α will be the dominant way for the doped Re atom to diffuse.

4. Conclusions

We have employed density functional theory calculations in conjunction with CI-NEB to study the vacancy formation and migration in clean and Re-doped Ni_3Al. The chemical potential of species and magnetism have been included to determine the vacancy formation energy. The evaluated average vacancy formation energy, $1.59\ \text{eV} < E^F_{av} < 1.64$ eV, compares well with the experimental result of 1.62 eV. We find that a localized magnetic moment is formed around vacancy V_β, which has explicitly decreased the formation energy of V_β; however, the influence of magnetism is much smaller for the formation of V_α.

The analysis of vacancy migration reveals that the migration of V_α within the α-sublattice is the most effective way for the diffusive motion of vacancies in Ni_3Al, and the evaluated activation energy is 2.6 eV, which is close to the experimental results of 3.0 eV. Accordingly, the diffusion of Ni atoms is likely to be mostly due to the migration of Ni atoms within their own sublattice (α-sublattice). However, Al atoms could not move freely within their own sublattice (β-sublattice), and it is also more effective for Al atoms using the α-sublattice for diffusion. By introducing a magnetic effect, we find that the magnetic moment decreases during the vacancy migration, which as a result elevates the energy barrier, and the mechanisms decreasing the magnetic moment are different between the V_α and V_β migrations.

With Re doping, while the formation of an Al vacancy is easier than in clean Ni_3Al, the formation of an Ni vacancy is slightly inhibited. The Re doping can also inhibit the migration of its neighbor vacancies. Based on the study of the diffusion of doped Re atoms, we find that Re_β is much more stable than Re_α, and the dominant way for doped Re to diffuse is by migration of the Re atom within the α-sublattice mediated by vacancies V_α.

Acknowledgement

This work was supported by '973' Project from the Ministry of Science and Technology of China (Grant No. 2006CB605102).

References

[1] Jackson JJ, Donachie MJ, Henrich RJ, Gell M. Metall Trans A 1977;8:1615.
[2] Gell M, Duhl DN, Giamei AF. In: Tien JK, Wlodek ST, Morrow III H, Gell M, Mauer GE, editors. Superalloys 1980: proceedings of the fourth international symposium on superalloys. Metals Park, OH: ASM; 1980. p. 205.
[3] Harris K, Erickson GL, Schwer RE. In: ASM International Handbook Committee, editor. Metals handbook. Properties and selection, vol. 1. Metals Park, OH: ASM; 1990. p. 995.
[4] Blavette D, Caron P, Khan T. In: Reichman S, Duhl D, Maurer G, Antolo-vich S, Lund C, editors. Superalloys 1988: proceedings of the sixth international symposium on superalloys. PA: Champion; 1988. p. 305.
[5] Herring C. J Appl Phys 1950;21:437.
[6] Weertman J, Weertman JR. In: Cahn RW, editor. Physical metallurgy. Amsterdam: North-Holland Publishing Co.; 1965. p. 793.
[7] Wang TM, Shimotomai M, Doyama M. J Phys F Metall Phys 1984;14:37.
[8] Dimitrov C, Zhang X, Dimitrov O. Acta Mater 1996;44:1691.
[9] Mehrer H. Diffusion in solids metals and alloys, vol. III. Landolt Börnstein; 1990.
[10] Shi Y, Frohberg G, Wever H. Phys Status Solidi A 1995;152:9657.
[11] Ikeda T, Almazouzi A, Numakura H, Koiwa M, Sprengel W, Nakajima H. Acta Mater 1998;46:5396.
[12] Cserháti C, Paul A, Kodentsov AA, Van Dal MJH, van Loo FJJ. Intermetallics 2003;11:291.
[13] Fu CL, Painter GS. Acta Mater 1997;43:481.
[14] Caro A, Victoria M, Averback RS. J Mater Res 1990;51:409.
[15] Gao F, Bacon DJ. Philos Mag 1993;67:275.
[16] Debiaggi SB, Decorte PM, Monti AM. Phys Status Solidi B 1996;195:37.
[17] Duan J. J Phys Condens Matter 2006;18:1381.
[18] Harris C, Tedstrom R, Daw MS, Mills MJ. Comput Mater Sci 2006;37:462.
[19] de Boer FR, Schinkel CJU, Biesterbos J, Proost S. J Appl Phys 1969;40:1049.
[20] Min BI, Freeman AJ, Jansen HJF. Phys Rev B 1988;37:6757.
[21] Kresse G, Hafner J. Phys Rev B 1993;47:558;
Kresse G, Furthmuller J. Phys Rev B 1996;54:11169.
[22] Blöchl PE. Phys Rev B 1994;50:17953;
Kresse G, Joubert D. Phys Rev B 1999;59:1758.
[23] Perdew JP. In: Ziesche P, Eschrig H, editors. Electronic structure of solids. Berlin: Akademie Verlag; 1991.
[24] Monkhorst HJ, Pack JD. Phys Rev B 1976;13:5188.
[25] Yoo MH. Acta Metall 1987;35:1559.
[26] Prikhodko SV, Carnes JD, Isaak DG, Yang H, Ardell AJ. Metall Mater Trans A 1999;30:2043.
[27] Henkelman G, Jóhannesson G, Jónsson H. In: Progress on theoretical chemistry and physics. Dordrecht: Kluwer Academic Publishers; 2000.
[28] Henkelman G, Uberuaga BP, Jónsson H. J Chem Phys 2000;113:9901.

[29] The implementations of the CI-NEB for VASP are obtained from: http://theory.cm.utexas.edu/henkelman.
[30] Erhart P, Albe K. Phys Rev B 2006;73:115207.
[31] Alahmed Z, Fu H. Phys Rev B 2007;76:224101.
[32] Wei SH, Zhang SB. Phys Rev B 2002;66:155211.
[33] Landau LD, Lifshitz EM. Statistical physics. 3rd ed. Oxford: Butterworth-Heinemann; 1980.
[34] Zhang SB, Northrup JE. Phys Rev Lett 1991;67:2339.
[35] Laks DB, Van de Walle CG, Neumark GF, Blochl PE, Pantelides ST. Phys Rev B 1992;45:10965.
[36] Cermak J. Comput Mater Sci 2002;25:606.
[37] Westbrook JH, Fleischer RL. In: Intermetallic compounds. Chichester: John Wiley & Sons; 1995.
[38] Kozubski R, Pfeiler W. Acta Mater 1996;44:1573.
[39] Hoshino K, Rothman SJ, Averback RS. Acta Metall 1988;36:1271.
[40] Numakura H, Ikeda T, Koiwa M, Almazouzi A. Philos Mag A 1998;77:887.
[41] Young WM, Elcock E. Proc Phys Soc 1966;89:735.
[42] Allnatt AR, Lidiard AB. Atomic transport in solids. Cambridge: Cambridge University Press; 2003.
[43] Besson R, Legris A, Morillo J. Phys Rev Lett 2002;89:225502.